Preprint of AIAA 2023-1874, presented at AIAA SCITECH, 23-27 January 2023, National Harbor, MD. https://doi.org/10.2514/6.2023-1874

Transverse Detonation Waves in Near-Limit Detonations

Mark D. Frederick*[1], Rohan M. Gejji†[1], Joseph E. Shepherd‡[2], and Carson D. Slabaugh§[1]
[1]*Purdue University, West Lafayette, IN 47907*
[2]*California Institute of Technology, Pasadena, CA 91125*

The occurrence of reactive transverse waves in a narrow channel are studied in stoichiometric mixtures of methane and oxygen with 40-45% nitrogen dilution. Schlieren and CH* chemiluminescence measurements are obtained at MHz rates to study dynamic features of the detonation. Observations are made regarding the different ways that reactive and detonative transverse waves appear. A specific instance of transverse detonation is quantitatively analyzed and it is found that the shocked gas upstream of the transverse detonation builds up until consumed by the transverse detonation. The speeds of the transverse detonation and leading high-speed shock, itself a detonation, are measured to be moving at U_{CJ} and $1.2U_{CJ}$, respectively.

I. Introduction

Spatial and temporal oscillations along the leading front of a detonation characterize the coupling between the gas-dynamic and chemical-kinetic aspects of the flow. In the classical cellular instability depiction of an unsupported detonation, the leading shock wave is attached to a reaction zone along high-speed portions of the front and the energy released in the reaction zone sustains the shock. The high-speed portions of the shock decay and eventually decouple from the reaction front due to unsteady effects [1] and transition into low-speed portions. Along these low-speed portions, gases that are processed by the shock may remain unreacted for some distance behind the front. Transverse waves originating at the junction of the high- and low-speed shocks move laterally along the leading shocks. Collision of transverse waves of opposite families create an explosion immediately behind the front that accelerates the leading wave, generating a new high-speed shock and transverse waves, resulting in quasi-periodic oscillation of the leading shock and the characteristic cellular pattern. This model can often be used to accurately describe weakly-unstable mixtures. However, as the detonation becomes more unstable the coupling between the shock and reaction front becomes more complex [2–4].

Of interest in this work is to understand what happens to the gas that is processed by the low-speed shock. Kiyanda and Higgins [5] experimentally estimated that in a stoichiometric methane-oxygen planar detonation, only 40-50% of reactants are processed by the high-speed shock and burn directly in an attached reaction front. The remainder must be processed by the low-speed shock and the reaction mechanism of this gas is an area of active study. In order for the average speed of the wave to remain at or near U_{CJ}, which has been shown to be the case in unstable mixtures [4], the gases that pass behind the low-speed shock must react and contribute to maintaining the average wave speed at a value consistent with complete reaction. The current theory is that these gases accumulate into regions or "pockets" that form along the shear layer between the high-speed shock and transverse wave. Upon collision of the transverse waves, these pockets detach from the front and exist as "unburned pockets" behind the front. The combustion mechanism of these remaining reactants is theorized to be primarily due to turbulent diffusive burning [6]. As long as the combustion of these pockets occurs before the pockets pass behind the sonic surface, which has been estimated to be to be about 4-7 cell-sizes (λ) downstream of the front [6, 7], the reactants are able to contribute to the wave. It has been observed in both experiments and simulations that unburned pockets exist and dissipate well within this 4-7 λ region [6].

The transverse wave plays an important role in consuming the reactants that persist behind the low-speed shock. Turbulence generated from the collision of transverse waves induces the necessary mixing for deflagrative burning of the unreacted pockets [8–10]. The transverse waves themselves may also be reactive, such as in the case of some weakly unstable mixtures [11]. Finally, and in the special case where the detonation is near-limit, the transverse wave may itself become a detonation, running through the shocked but unburned gas attached to the low-speed shock. This was first observed by Strehlow and Crooker [12] in a rectangular channel with a mixture of hydrogen/oxygen/argon at low pressure. Since then, transverse detonations are often observed experimentally in geometries designed to bring the detonation

*Graduate Research Assistant, School of Mechanical Engineering, AIAA Student Member
†Research Engineer, School of Aeronautics and Astronautics, AIAA Senior Member
‡C. L."Kelly" Johnson Professor of Aeronautics and Mechanical Engineering, Graduate Aerospace Laboratories
§Associate Professor, School of Aeronautics and Astronautics, AIAA Associate Fellow

near the limit of self-sustained propagation, such as through divergent channels [13], diffraction [14, 15], porous media [16], and lateral strain [17, 18]. Numerous simulation have also been performed on the topic [13, 15, 16, 19]. Most recently, simulations by Floring *et al.* [20], modeling the experiment of Bhattacharjee *et al.* [15], have reported on the initiation mechanism of transverse detonation and that the speed of the transverse detonation is indeed moving at U_{CJ}, a result that will be experimentally confirmed here.

In this work we use a narrow detonation channel to examine mixtures of methane/oxygen/nitrogen that exhibit reactive and detonative transverse waves. Images of the gas-dynamic and chemical-kinetic fields are acquired at MHz rates and with high spatial resolution to allow for flow dynamics to be quantified. We examine the state of the gas immediately downstream of the low-speed shock to determine conditions that the transverse wave is running through. This approach allows for the quantification and comparison of the speeds of the primary shocks in the transverse detonation wave system.

II. Experiment Description

A. Detonation Channel

The *Narrow Channel Facility* (NCF) was developed by Austin[21] in the Explosion Dynamics Laboratory at Caltech to study the unstable structure in gaseous detonations. The NCF is a high aspect ratio, rectangular channel with a height of 152.4 mm width of 17.8 mm, and span of 4.2 m. The dimensions were chosen such that the width is nominally smaller than the detonation cell size for a targeted range of mixtures and test conditions. This configuration effectively suppresses transverse wave motion across the width of the channel, generating a two-dimensional detonation structure across the channel height that is conducive to the application of path-integrated optical diagnostics.

The reactant gases, typically an oxidizer, an inert, and one or two fuels, are introduced into the channel using the method of partial pressures. The loading process takes approximately 120 seconds and the reactants are circulated for an additional thirty seconds to ensure a homogeneous mixture. A K-type thermocouple and low frequency pressure transducer are placed just upstream of the branched initiator and are used to record the initial temperature and pressure. The planar detonation is driven by a branched initiator, designed by Jackson and Shepherd[22]. The initiator operates with an equimolar C_2H_2-O_2 mixture and is ignited with a spark plug. The facility is operated at low pressure ($\approx$ 20 kPa) to produce large structures that are amenable to observation with imaging diagnostics.

Pressure fluctuations in the channel are recorded at six axially distributed locations using PCB 113B26 high-frequency dynamic pressure transducers (PT), installed flush with the channel wall, and sampled at 2 MHz. PT 1-3 monitor the planarity of the wave as it enters the test section. PT 4-8 are used to track the progression of the detonation wave as it traverses the channel by using the time of arrival method. These data can be used to monitor the detonation velocity and compare with the theoretical Chapman Jouguet velocity. Figure 1 identifies the location of all the high-frequency pressure measurement locations (PT 1-8). More details on the experimental procedure are available in Frederick *et al.* [23, 24].

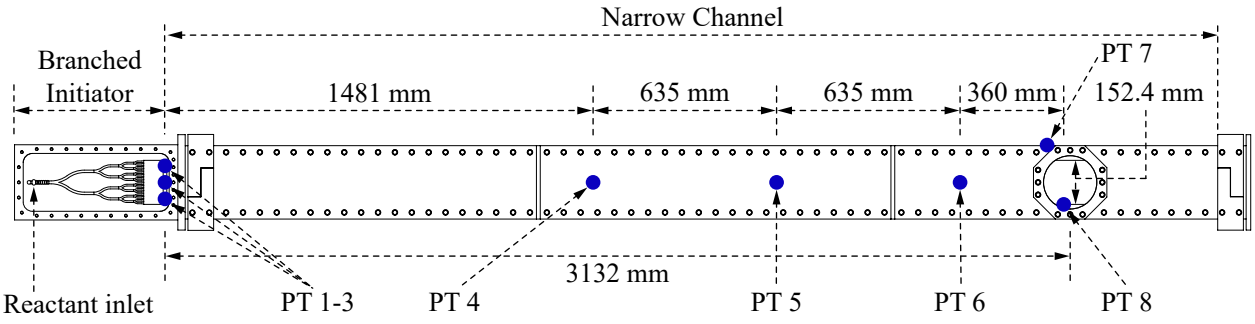

Fig. 1 Experimental overview and dimensions. High frequency pressure measurement locations labeled as PT 1-8.

B. Diagnostics

Two different diagnostic configurations were used in this work. Both utilize the optical access provided by 170 mm fused quartz windows located at the end of the channel, shown in figure 1. The first configuration is an inline lens-type schlieren system, which was used to capture the images shown in Fig. 3. A pulsed LED is used as the light-source. The LED produces an incoherent 635 ± 7 nm light with a 110 ns pulse duration at a 5 MHz pulse frequency. An aspheric condenser lens is placed directly downstream of the light source and passes the focus of the beam through an aperture to enforce a point source. A 250 mm lens is used to collimate the light through the test section and a 500 mm lens is used to collect the light and focus it onto the schlieren cutoff, which is a circular aperture. The light passes through a 631/21 nm single-band bandpass filter to eliminate light emission from the detonation. 128 images are record at a rate of 5 MHz on a Shimadzu HPV-X2 high-speed camera with a 150 mm custom camera lens. The Shimadzu HPV-X2 detector has a sensor size of 400 x 250 pixels. The field of view was 57.32 x 35.77 mm, yielding a spatial resolution of 143.2 $\mu m/px$.

The second diagnostic configuration, shown schematically in Figure 2, utilized two Shimadzu HPV-X2 cameras to perform simultaneous schlieren and CH* chemiluminescence imaging at a rate of 1.66 MHz. The images obtained from this setup are shown in Fig. 4. For the schlieren configuration f/10 parabolic mirrors are used instead of the lenses used in the inline configuration. The exposure time of the schlieren camera was 200 ns. The CH* chemiluminescence ($A^2X \rightarrow X^2\Pi_r$) was recorded on a camera placed beneath the schlieren beam path, angled at 9° to have a coincident field of view with the schlieren camera. A 434/17nm (Semrock 434/17 BrightLine) single-band band-pass filter was used to collect the CH* signal. The exposure time of the chemiluminescence camera was 300 ns. The field of view obtained by this configuration is larger than configuration one, at 133 x 83 mm, depicted in figure 2. The resulting spatial spatial resolution is 352.1 $\mu m/px$. The cameras both record 128 images per test.

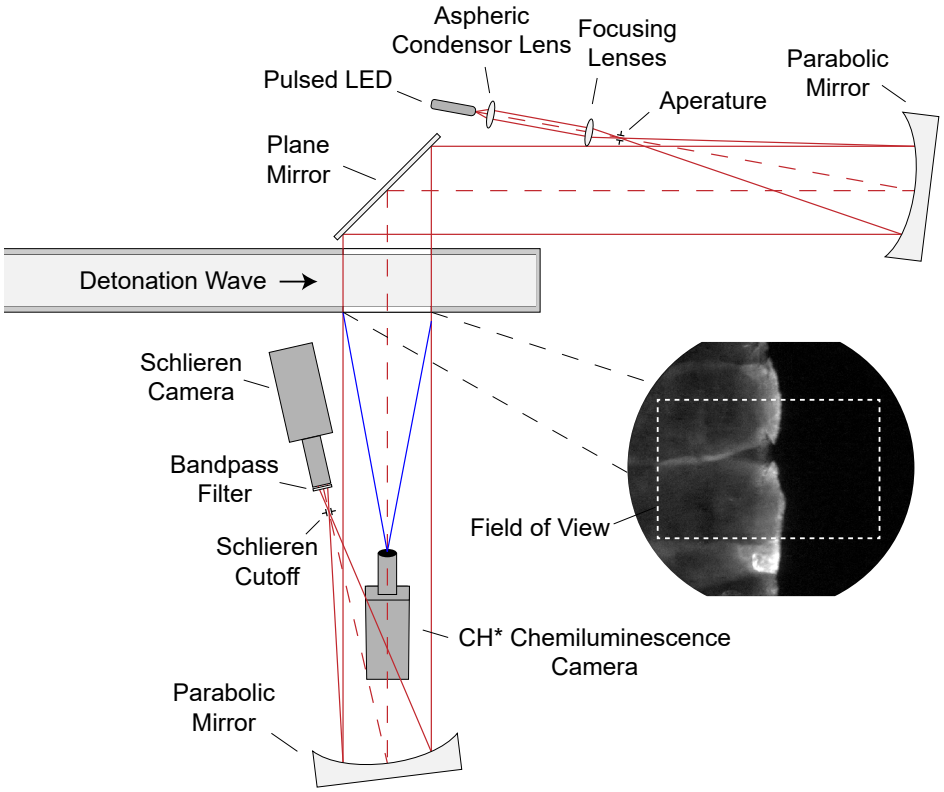

Fig. 2 Schematic illustration of optical setup for simultaneous Z-type schlieren and broadband imaging measurements. Not to scale. The image illustrating the field of view is of CH* chemiluminescence from a methane detonation.

III. Results

In order to produce flow-fields that manifest a transverse detonation wave, mixtures of stoichiometric methane and oxygen diluted with 40% and 45% of nitrogen by volume were examined. This level of dilution is the limit of what we have been able to consistently detonate in the NCF. Table 1 list the initial conditions and calculated detonation parameters for the four cases studied. All cases were initiated near the same initial pressure and temperature.

Table 1 Calculated detonation parameters. U_{CJ} is the Chapman-Jouguet velocity, M_{CJ} is the Mach number, Δ_I is the induction length, Δ_E is the exothermic length. All parameters are found using ZND calculations in the Shock and Detonation Toolbox [25] with the GRI3.0 reaction mechanism [26].

Case	Mixture	P_0 [kPa]	T_0 [K]	P_{vN} [MPa]	T_{vN} [K]	U_{CJ} [m/s]	M_{CJ}	Δ_I [mm]	Δ_E [mm]
a	CH_4-$2O_2$-$2N_2$	20.79	299	0.85	1692	2059	5.81	5.37	0.183
b	CH_4-$2O_2$-$2N_2$	20.85	299	0.85	1692	2059	5.81	5.35	0.183
c	CH_4-$2O_2$-$2.5N_2$	19.33	294.5	0.77	1665	2018	5.74	7.85	0.231
d	CH_4-$2O_2$-$2.5N_2$	20.78	294.5	0.83	1667	2020	5.75	7.24	0.215

A. Regimes of transverse wave reactivity

A select number of images captured for cases (a) and (b) are shown in the left and right column of Figure 3, respectively. Only schlieren imaging was performed for these cases and 5 of the 128 images captured for each case are included. Background subtraction is performed to remove stationary gradients introduced by imperfections in the windows. These images capture a variety of ways in which a transverse wave may appear in highly unstable mixtures. Case (a), shown in the left column of Fig. 3, depicts the second-half of the cycle of cellular detonation propagation. Frame (a) shows a high-speed shock (HS) entering from the top of the frame along with the triple-point (TP) that joins the high-speed shock, the low-speed shock (LS), which spans the height of the image, and the transverse wave (TW), which extends behind the shock front. In frame (b) a second transverse wave with a triple-point structure resembling a Mach reflection enters from the bottom of the frame. These two families of waves move toward each other and collide (just after frame (e)). The collision of the transverse waves at this point generates a new high-speed shock (not captured) that marks that beginning of a new cellular cycle.

In the following discussion we will speculate about the reactivity of the transverse waves and other flow features based only on the schlieren images. Schlieren is only a measurement of the density gradient and does not capture the reaction field directly. Our interpretation of the reaction progress and intensity from schlieren is based on the results of Pintgen *et al.* [27] and Austin *et al.* [28], who performed simultaneous single-shot OH planar laser induced and schlieren, as well as in the simultaneous schlieren and chemiluminescence measurements of Frederick *et al.* [4, 24] and of Kiyanda and Higgens [5]. Our analysis of these previous results generally leads us to believe that larger density gradients, which appear as darker regions in the images, correspond to regions of intense reaction.

Of particular interest in case (a) is the reactivity of the two transverse waves, which are called out in frame (b) of Fig. 3 as (i) and (ii). The reactants that are upstream of the transverse waves are between the low-speed shock and feature (iii), which is either a weak reaction front or a contact surface separating the reactants from the remnants of a now quenched reaction front. The gas that is between (LS) and (iii) in frame (c) remains unreacted after being processed by the low-speed shock and will be referred to as the "shocked but unreacted" region for the remainder of this paper. As transverse wave (i) moves through the shocked but unreacted gas region it appears to partially react the gas within because the wave (i) is dark and wrinkled, indicating reaction. However, there is a region of gas (feature iv) that makes it downstream of (i) and appears as a distributed perturbation in the density field, which is likely unreacted gas. Upon transverse wave collision, region (iv) will detach from the front completely and become an "unreacted gas pocket", which has been discussed in many studies [5, 6, 28–32]. The lower transverse wave (ii) has a different character as it moves through the shocked but unreacted region as compared to (i). It is much darker and very little unreacted gas makes it downstream. This suggests that the wave is at least more reactive than (i) and is possibly propagating as a detonation.

Case (b), shown in the right column of Fig. 3, shows another example of what is likely a reactive transverse wave. Once again, at the beginning of this case (frame f) the height of the frame is spanned by a low-speed shock with an attached shocked but unreacted region. Also of note in frame (f) is the appearance of an apparent "double" low-speed shock, which is due to three dimensional effects in the channel [21]. A weak transverse wave and associated triple point, feature (vi), is also present. Behind the shocked but unreacted region there is a volume of unreacted gas (v),

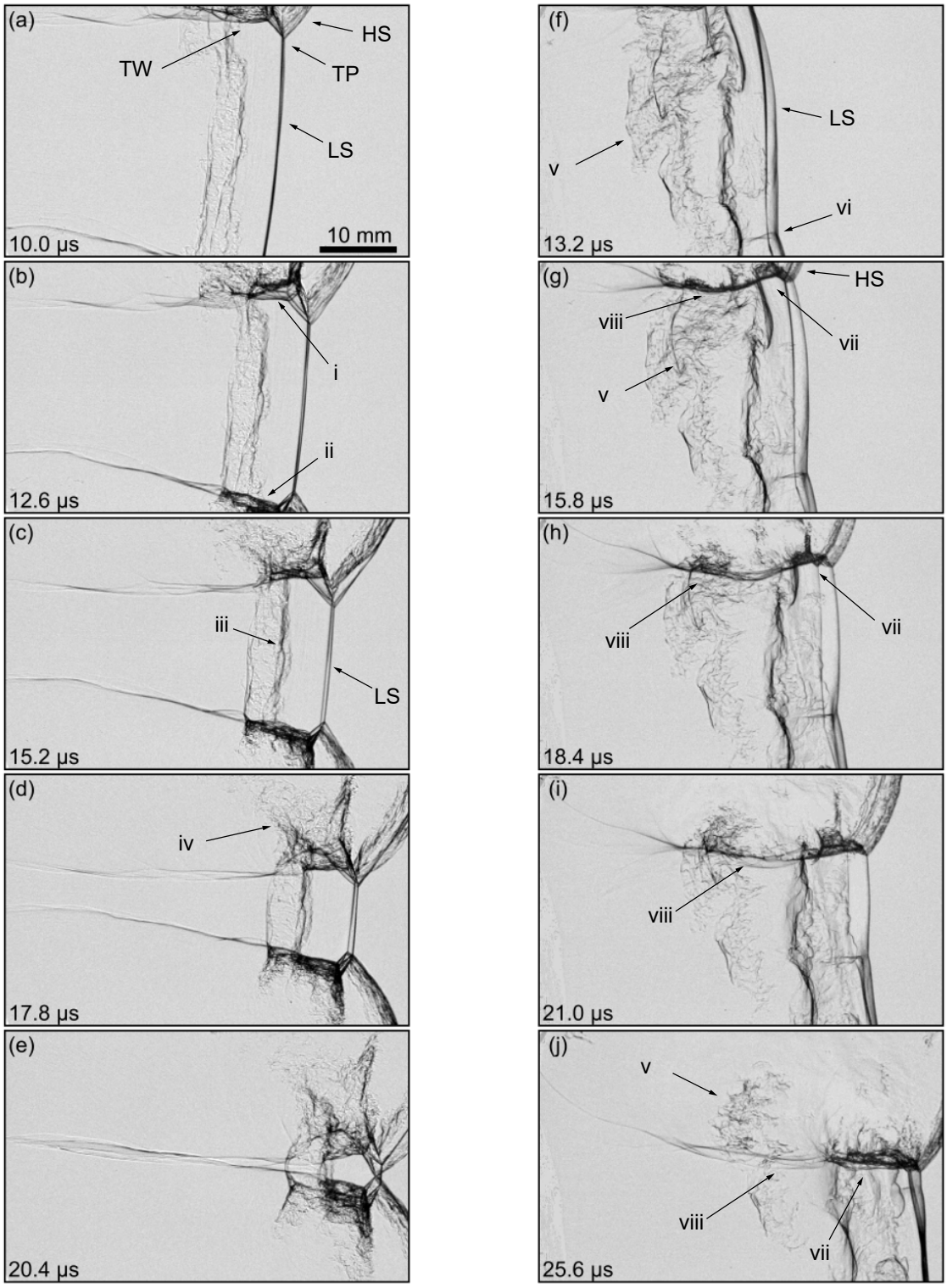

Fig. 3 Sequence of select schlieren images showing case (a) in the left column and case (b) in the right column. Key features are called out as: HS: high-speed shock, LS: low-speed shock, TP: triple-point, TW: transverse-wave. Additional callouts are described in the text.

similar in appearance to feature (iv), that exists to a larger extent in the top half of the frame than in the bottom. In frame (g) a high-speed shock (HS) and transverse wave enter the image. The transverse wave can be separated into two parts: a section within the shocked but unreacted region attached to the low-speed shock (vii) and a section within the unreacted gas-pocket (viii), immediately behind the shocked but unreacted region. Section (vii) remains dark, and is likely reactive, throughout the entire case (through frame j) as it moves through the shocked but unreacted region. The structure of the triple point in this region resembles that of a double Mach reflection [33]. The density fluctuations behind (vii) in frame (j) quickly becomes homogeneous, with only small pockets of what is probably unreacted gas remaining. In contrast, the reactivity of transverse wave section (viii) changes as the case progresses. In frame (g) the wave is dark, indicating reaction, and consumes much of the unburned gas pockets (v) ahead of it. By frame (j) the transverse wave appears lighter, indicating no reaction, and the gas pockets (v) are still present despite being processed by the transverse wave. These multiple modes of transverse wave reactivity all represent different mechanisms by which reactants may or may not be processed behind the front. Our interpretation of these schlieren images will be supported by more concrete evidence enabled by the CH* chemiluminescence images discussed in the next section.

B. Particle Path Analysis

The cases shown in Figure 4, (c) and (d), were imaged using simultaneous schlieren and CH* chemiluminescence. The combination of these two diagnostics allows for an analysis of the coupled gas-dynamic and chemical-kinetic fields. A select number of frames from each case is shown along with a map of the leading front normal velocity (frames e and j). The velocity maps are generated by extracting the leading edge from each schlieren image in time and computing the velocity using a second order finite difference method. The dotted lines shown on the velocity maps correspond to the leading fronts of the displayed images. These maps quantify the velocity oscillation throughout a cell cycle or portion thereof. Further details on the velocity computation can be found in [4]. A statistical representation of the lead shock velocity in time is displayed in the histograms of Figure 5. The velocity contributions from the high- and low-speed shocks are displayed in red and blue, respectively.

Cases (c) and (d) were taken at nearly the same initial condition (see Table 1), and like cases (a) and (b), manifest distinct regimes of transverse wave reactivity. Case (c), shown in the left column of Fig. 4 has a low-speed speed shock that is traveling at an average speed of $0.77U_{CJ}$, which is the average value of the low-speed shock peak (blue) in Fig. 5a. The region immediately downstream of the low-speed shock remains unreacted. At frame (b) a triple point structure resembling simple Mach reflection is associated with a transverse wave entering from the bottom of the frame. The high-speed leading shock associated with this triple point is travelling at an average speed of $0.91U_{CJ}$. The reaction following the high-speed shock decouples from it as the case progresses in time. Within the shocked but unreacted region, the transverse wave is non-reactive based on the lack of trailing chemiluminescence. However, the transverse wave downstream of the contact surface does produce a chemiluminescence signal. It is not immediately clear what is causing this because the transverse wave does not move through any visible unreacted pockets (such as feature (v) in Fig. 3g). It is our hypothesis that the chemiluminescence signal produced behind the transverse wave is caused by the excitation of ground-state CH that exists following the decoupling of the wave that now appears as the low-speed shock. The decoupling event, which took place before image acquisition began, occurs when the propelling effects caused by energy release from the reactants can no longer complete with the retarding effects of the expansion behind the wave. At the moment of decoupling the pressure and temperature drop sharply, freezing any chemical reactions in progress. Following decoupling, only very slow chemical reaction occurs, as evidenced by the gradual chemiluminescence decay in the downstream region of frames (a) - (c). When the transverse wave passes, the frozen intermediate species are brought to a higher temperature and pressure, causing the remaining ground state CH molecules to be excited to a higher electronic level and produce a chemiluminescence signal upon relaxation. A detailed reaction analysis is needed to validate this hypothesis and will be the subject of future work.

Case (d) (right column of Fig. 4), like case (c), begins in frame (f) with a low-speed shock that extends the height of the frame and is moving with an average speed of $0.76U_{CJ}$. However, unlike case (c), the feature that enters the field-of-view, in frame (g), is a transverse detonation, where both the high-speed shock and transverse wave are detonative. The high-speed shock is overdriven, with an average speed of $1.11U_{CJ}$. We will quantify the designation of "detonation" for the transverse wave in section III.C. Both the high-speed shock and transverse wave are reactive to such a degree that the emitted chemiluminescence signal appears ahead of the shocks. This is not a physical manifestation, rather the chemiluminescence intensity is so high that it "bleeds" into neighboring parts of the image. In Fig. 7 the chemiluminescence can be seen in the schlieren image as well. The gas-dynamic field immediately downstream of high-speed shock and transverse detonation is uniform, suggesting that all gases that are processed by these shocks is

consumed completely.

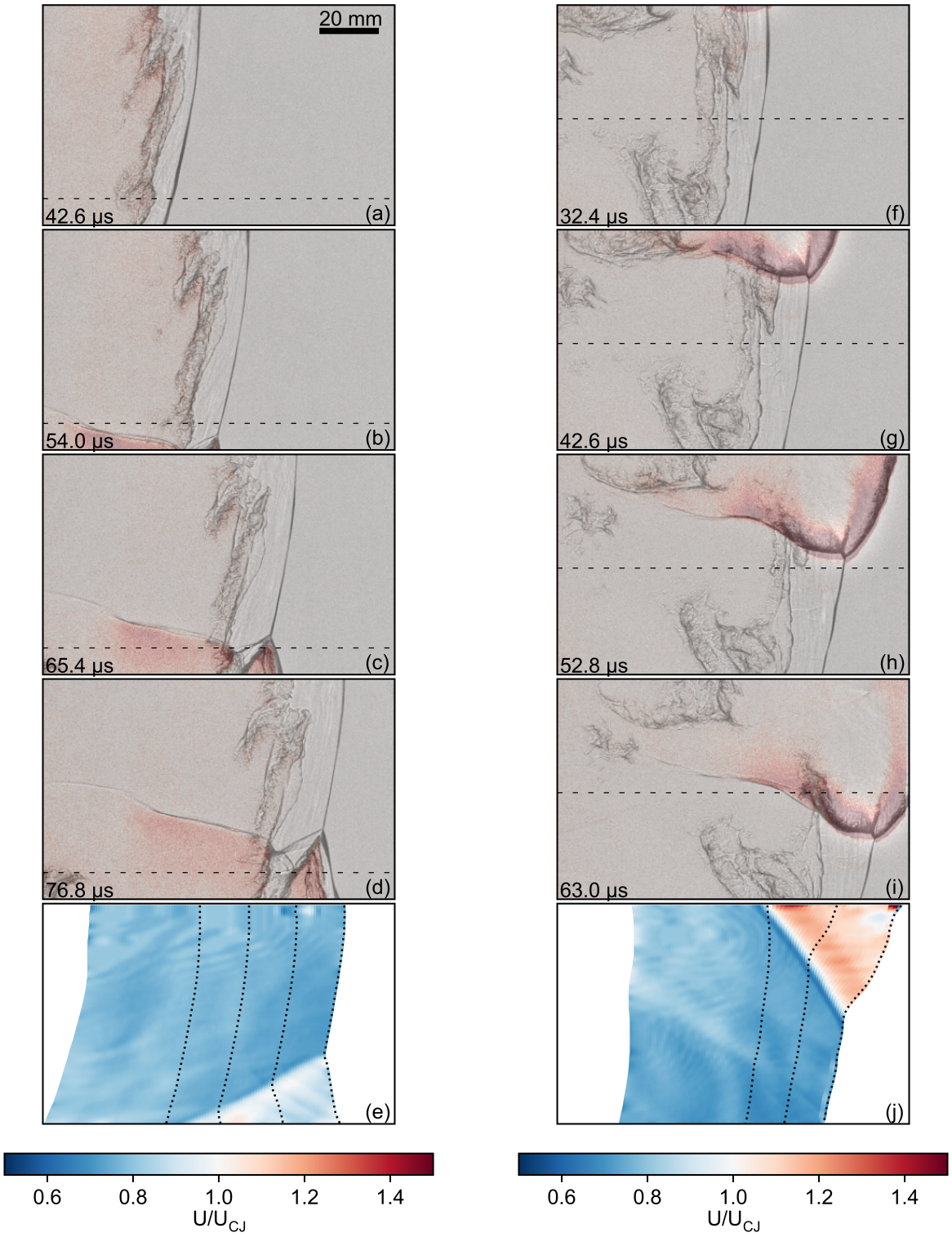

Fig. 4 Sequence of schlieren images of CH_4-$2O_2$-$2.5N_2$ detonations. Case (c) is shown in frames (a-e) and case (d) is shown in frame(f-j). The dotted line overlaid on each frame corresponds to the selected region in Fig. 6. Leading shock front velocity maps are included in frames (e) and (j).

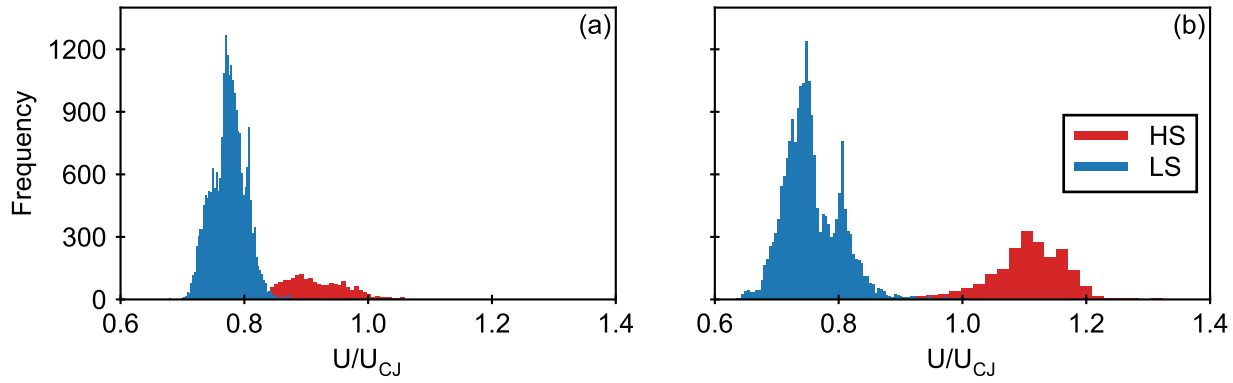

Fig. 5 Histogram of leading shock normal velocity for case (c) is shown in the left column and (d) in the right column. The measured velocities from the high-speed shock (HS) are shown in red and the low-speed shock (LS) in blue.

In order to understand the state of the gas that the transverse waves move through, an analysis of particle paths in the region immediately behind the low-speed shock is required. Figure 6 shows x-t diagrams taken at the horizontal slices indicated by the dashed lines shown in Fig. 4. This is done for both case (c) and (d) in the left and right columns of Fig. 6, respectively. In these x-t diagrams the schlieren and chemiluminescence signals are both represented. Above a certain threshold the schlieren signal is binarized and represented in gray. The chemiluminescence signal is overlaid in red. The slope of the rightmost schlieren trace (gray line) corresponds the the leading shock speed. When the high-speed portion of the leading front crosses the horizontal slice coordinate (61 μs for case (c) and 54 μs for case (d)) the slope of the rightmost schlieren trace rapidly steepens to reflect the increased speed of the high-speed shock.

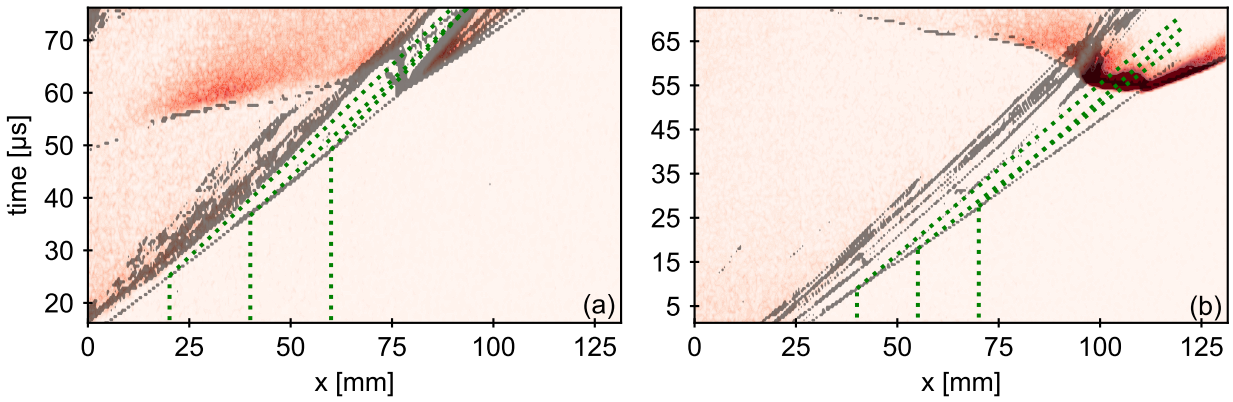

Fig. 6 x-t diagrams showing estimated particle trajectories for cases (c) and (d), respectively. The y-location of the cuts is shown as a dashed line in Fig. 4.

During the low-speed portion of the shock front captured in the x-t diagram three particle-paths at distinct x-coordinates are estimated for each case. The particle-paths are represented by green dotted lines and are estimated by assuming that once the particle is processed by the the leading shock no reactions take place and it remains chemically frozen. This assumption is justified by the lack of chemiluminescence signal immediately behind the low-speed shock. The induced speed (in the laboratory frame of reference) U_2 imposed on the particle by the shock is then calculated by

$$U_2 = W - w_2$$

where W is the measured shock speed and from continuity the induced velocity in the shock attached reference frame w_2 is

$$w_2 = \frac{\rho_1 w_1}{\rho_2}$$

and the post shock density ρ_2 is found using the *postshock_fr* routine in the Shock and Detonation Toolbox[25]. For neither case shown in Fig. 6 do the particle paths escape the shocked but unreacted region and cross into the contact

surface that is wrinkled in the schlieren images and has very weak, if any, chemiluminescence intensity. Additionally, the induction time (computed with the constant pressure model) of a particle crossing the low-speed shock at $0.76U_{CJ}$ (mean speed from histogram) of case (d) is 8.42 ms. The induction time of the particle is two orders of magnitude larger than the transit time to the transverse detonation, indicating that little to no reaction occurs in transit. This means that gas processed by the low-speed shock for these cases builds up and, in the instance of case (d) (frame (b) of Fig. 6), only reacts when the transverse detonation, which is fed by this unburned gas, moves through it. For case (c) (frame (a) of Fig. 6) the gas collects in the region downstream of the high-speed shock and transverse wave. Although this is not captured, it likely breaks off from the main front upon transverse wave collision and forms an unreacted gas pocket.

C. Shock Speed Analysis

To support our claim that the transverse wave in case (d) is a detonation, the speed of the transverse wave is computed and compared to U_{CJ} of the gas within the shocked but unreacted region. The first step in performing this analysis is to extract the location of the transverse wave. Figure 7(a) shows a single schlieren image of case (d) with the extracted transverse wave location shown in green, along with the high-speed shock in red, the low-speed shock in blue, and the triple-point in yellow. The transverse wave is extracted for all frames in time in a method similar to the leading edge (see section III.B). The spatial coordinates of the extracted transverse wave are shown in Fig. 7(b) and are presented in a reference frame attached to the triple-point, where $x = 0$ corresponds to the triple-point location. A velocity-map, shown in Fig. 7(c), is computed along the y-direction of the extracted edges with a second-order finite-difference method. The velocity of the transverse wave remains relatively constant in time and space, slightly accelerating in the top of the frame and with some low speed fluctuations in the downstream portion due to errors in edge detection.

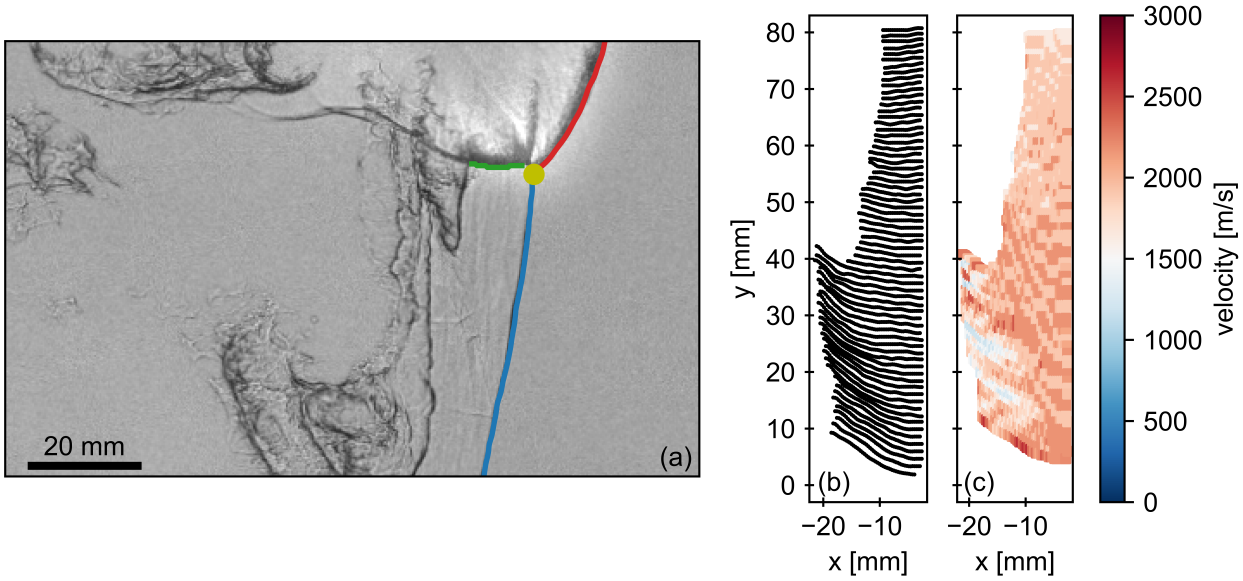

Fig. 7 (a) Schlieren image of case (d) highlighting the three primary waves: high-speed shock: red, low-speed shock: blue, and transverse detonation: green. (b) The spatial coordinates of the extracted transverse detonation and (c) the velocity map of the transverse detonation in the reference frame of the triple-point. The coordinate $x = 0$ corresponds to the triple-point location.

Time traces of normalized velocity for a point on each shock taken near the triple-point are plotted in Figure 8. Each shock is normalized by U_{CJ} for the mixture it is moving through. For the high- and low-speed shocks the initial mixture conditions are used. For the transverse wave it is assumed that the gas state behind the low-speed shock is frozen. The post-shock state is calculated with the measured low-speed shock speed and used to compute U_{CJ} of the shocked but unreacted gas, which is 2039 m/s. Applying this normalization, it becomes apparent that the transverse wave moves at or near U_{CJ} for the duration of the test, confirming that this wave is indeed a Chapman-Jouguet detonation. A similar result has recently been obtained in the simulations performed by Floring *et al.* [20].The low-speed shock is under-driven, moving at an average speed of $0.71U_{CJ}$. The high-speed shock travels at a near constant speed, with an average of $1.18U_{CJ}$. Unlike the typical overdriven portion of a detonation front that occurs following transverse wave collision, the

high-speed shock here does not rapidly decay. This is a result the rapid rate of energy release behind both detonative waves and can be quantified by considering the the very small induction times of particles that are processed by each wave. The induction time of the high-speed and transverse detonations, computed at the average speeds reported above, are 1.45 μs and 0.28 μs, respectively. Compared to the induction time of a wave moving at U_{CJ} through the initial mixture, which is 24.0 μs, the high-speed and transverse detonations have induction times that are 16.6 and 85.7 times smaller, respectively. Because of this very rapid and short reaction zone length, the expansion due to transverse and lateral gradients behind the wave does not compete with the reaction and the wave speeds do not noticeably decay.

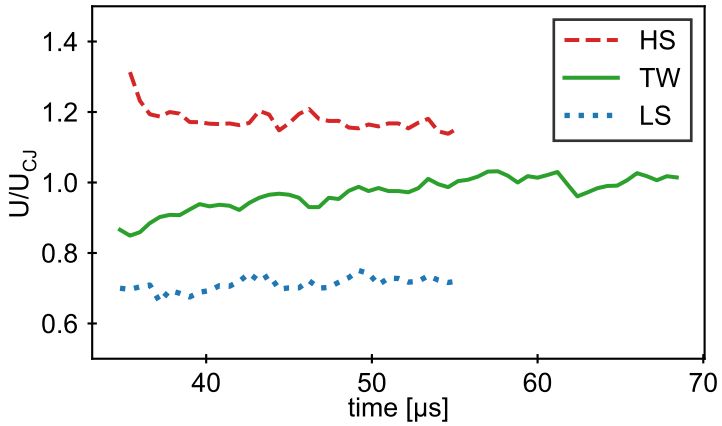

Fig. 8 The normalized shock speed (U/U_{CJ}) of the high-speed shock (red), transverse detonation (green), and low-speed shock (blue).

IV. Conclusion

In this work we studied the transverse wave characteristics that manifest in highly unstable mixtures of methane, oxygen, and nitrogen using MHz rate schlieren and CH* chemiluminescence. Different regimes of transverse wave reactivity were observed, from a nonreactive wave to a transverse detonation. In one occurrence the transverse wave is seen to burn unreacted gas pockets, providing another mechanism by which reactants are consumed. We determined that particles processed by the low-speed shock in these mixtures build up in the shocked but unreacted region and only react along the front when consumed by a transverse detonation. Finally, measurements of shock speeds in the presence of a transverse detonation confirmed that the transverse wave is a Chapman Jouguet detonation.

Acknowledgments

This work was supported by U.S. Air Force Office of Scientific Research grant FA9550-21-1-0013 (PO: Dr. Chiping Li). Mark D. Frederick acknowledges support from the National Science Foundation Graduate Research Fellowship Program under Grant No. DGE-1333468. One Shimadzu HPV-X2 used in this work was purchased with DURIP grant FA9550-20-1-0226 (PO: Dr. Chiping Li). The authors are grateful to Hadland Imaging for use of the second Shimadzu HPV-X2.

References

[1] Eckett, C. A., Quirk, J. J., and Shepherd, J. E., "The role of unsteadiness in direct initiation of gaseous detonations," *Journal of Fluid Mechanics*, Vol. 421, 2000, pp. 147–183. https://doi.org/10.1017/S0022112000001555.

[2] Austin, J., and Shepherd, J., "Detonations in hydrocarbon fuel blends," *Combustion and Flame*, Vol. 132, No. 1, 2003, pp. 73–90. https://doi.org/10.1016/S0010-2180(02)00422-4.

[3] Shepherd, J., "Detonation in gases," *Proceedings of the Combustion Institute*, Vol. 32, No. 1, 2009, pp. 83–98. https://doi.org/10.1016/j.proci.2008.08.006.

[4] Frederick, M. D., Gejji, R. M., Shepherd, J. E., and Slabaugh, C. D., "Statistical analysis of detonation wave structure," *Proceedings of the Combustion Institute*, 2022. https://doi.org/10.1016/J.PROCI.2022.08.054.

[5] Kiyanda, C. B., and Higgins, A. J., "Photographic investigation into the mechanism of combustion in irregular detonation waves," *Shock Waves*, Vol. 23, 2013, pp. 115–130. https://doi.org/10.1007/s00193-012-0413-8.

[6] Radulescu, M. I., Sharpe, G. J., Law, C. K., and Lee, J. H. S., "The hydrodynamic structure of unstable cellular detonations," *Journal of Fluid Mechanics*, Vol. 580, 2007, p. 31–81. https://doi.org/10.1017/S0022112007005046.

[7] Edwards, D. H., Jones, A. T., and Phillips, D. E., "The location of the Chapman-Jouguet surface in a multiheaded detonation wave," *Journal of Physics D: Applied Physics*, Vol. 9, No. 9, 1976, pp. 1331–1342. https://doi.org/10.1088/0022-3727/9/9/010.

[8] Radulescu, M. I., and Lee, J. H., "The failure mechanism of gaseous detonations: Experiments in porous wall tubes," *Combustion and Flame*, Vol. 131, No. 1-2, 2002, pp. 29–46. https://doi.org/10.1016/S0010-2180(02)00390-5.

[9] Lau-Chapdelaine, S. S., Xiao, Q., and Radulescu, M. I., "Viscous jetting and Mach stem bifurcation in shock reflections: Experiments and simulations," *Journal of Fluid Mechanics*, Vol. 908, No. 1986, 2020. https://doi.org/10.1017/jfm.2020.731.

[10] Sow, A., Lau-Chapdelaine, S. M., and Radulescu, M. I., "The effect of the polytropic index γ on the structure of gaseous detonations," *Proceedings of the Combustion Institute*, Vol. 38, No. 3, 2021, pp. 3633–3640. https://doi.org/10.1016/j.proci.2020.07.067.

[11] Subbotin, V., "Collision of transverse detonation waves in gases," *Combustion, Explosion, and Shock Waves*, Vol. 11, No. 3, 1975, pp. 411–414. https://doi.org/10.1007/BF00740553.

[12] Strehlow, R. A., and Crooker, A. J., "The structure of marginal detonation waves," *Acta Astronautica*, Vol. 1, No. 3-4, 1974, pp. 303–315. https://doi.org/10.1016/0094-5765(74)90100-3.

[13] Gamezo, V. N., Vasil'ev, A. A., Khokhlov, A. M., and Oran, E. S., "Fine cellular structures produced by marginal detonations," *Proceedings of the Combustion Institute*, Vol. 28, No. 1, 2000, pp. 611–617. https://doi.org/10.1016/S0082-0784(00)80261-1.

[14] Pintgen, F., and Shepherd, J. E., "Detonation diffraction in gases," *Combustion and Flame*, Vol. 156, 2009, pp. 665–677. https://doi.org/10.1016/j.combustflame.2008.09.008.

[15] Bhattacharjee, R. R., Lau-Chapdelaine, S. S., Maines, G., Maley, L., and Radulescu, M. I., "Detonation re-initiation mechanism following the Mach reflection of a quenched detonation," *Proceedings of the Combustion Institute*, Vol. 34, No. 2, 2013, pp. 1893–1901. https://doi.org/10.1016/J.PROCI.2012.07.063.

[16] Radulescu, M. I., and Maxwell, B. M. N., "The mechanism of detonation attenuation by a porous medium and its subsequent re-initiation," *Journal of Fluid Mechanics*, Vol. 667, 2011, pp. 96–134. https://doi.org/10.1017/S0022112010004386.

[17] Xiao, Q., and Radulescu, M. I., "Dynamics of hydrogen–oxygen–argon cellular detonations with a constant mean lateral strain rate," *Combustion and Flame*, Vol. 215, 2020, pp. 437–457. https://doi.org/10.1016/j.combustflame.2020.01.041.

[18] Xiao, Q., and Radulescu, M. I., "Role of instability on the limits of laterally strained detonation waves," *Combustion and Flame*, Vol. 220, 2020, pp. 410–428. https://doi.org/10.1016/J.COMBUSTFLAME.2020.06.040.

[19] Han, W., Wang, C., and Law, C. K., "Role of transversal concentration gradient in detonation propagation," *Journal of Fluid Mechanics*, Vol. 865, 2019, pp. 602–649. https://doi.org/10.1017/jfm.2019.37.

[20] Floring, G., Peswani, M., and Maxwell, B., "On the role of transverse detonation waves in the re-establishment of attenuated detonations in methane–oxygen," *Combustion and Flame*, Vol. 247, 2023. https://doi.org/10.1016/J.COMBUSTFLAME.2022.112497.

[21] Austin, J. M., "The role of instability in gaseous detonation," Ph.D. thesis, California Institute of Technology, 2003. https://doi.org/10.7907/X7YH-T687.

[22] Jackson, S. I., Austin, J. M., and Shepherd, J. E., "Planar detonation wave initiation in large-aspect-ratio channels," *AIAA Journal*, Vol. 44, No. 10, 2006, pp. 2422–2425. https://doi.org/10.2514/1.21581.

[23] Frederick, M. D., Gejji, R. M., Shepherd, J. E., and Slabaugh, C. D., "Preliminary Results from Narrow Channel Facility Experiments at Purdue University," *AIAA Propulsion and Energy Forum*, 2019, pp. 1–8. https://doi.org/10.2514/6.2019-4218.

[24] Frederick, M. D., Gejji, R. M., Shepherd, J. E., and Slabaugh, C. D., "Time-resolved imaging of the cellular structure of methane and natural gas detonations," *Shock Waves*, Vol. 32, 2022, pp. 337–351. https://doi.org/10.1007/s00193-022-01080-8.

[25] Shepherd, J., "Shock and Detonation Toolbox," , 2018. URL https://shepherd.caltech.edu/EDL/PublicResources/sdt/.

[26] Smith, G. P., Golden, D. M., Frenklach, M., Moriarty, M. W., Eiteneer, B., Goldenberg, M., Bowman, C. T., Hanson, R. K., Song, S., Gardiner, W. C., Lissianski, V. V., and Qin, Z., "GRI-Mech," , Jul. 1999. URL www.me.berkeley.edu/gri_mech/.

[27] Pintgen, F., Eckett, C., Austin, J., and Shepherd, J., "Direct observations of reaction zone structure in propagating detonations," *Combustion and Flame*, Vol. 133, No. 3, 2003, pp. 211–229. https://doi.org/10.1016/S0010-2180(02)00458-3.

[28] Austin, J., Pintgen, F., and Shepherd, J., "Reaction zones in highly unstable detonations," *Proceedings of the Combustion Institute*, Vol. 30, No. 2, 2005, pp. 1849–1857. https://doi.org/10.1016/j.proci.2004.08.157.

[29] Oran, E. S., Young, T. R., Boris, J. P., Picone, J. M., and Edwards, D. H., "A study of detonation structure: The formation of unreacted gas pockets," *Symposium (International) on Combustion*, Vol. 19, No. 1, 1982, pp. 573–582. https://doi.org/10.1016/S0082-0784(82)80231-2.

[30] Mahmoudi, Y., and Mazaheri, K., "High resolution numerical simulation of triple point collision and origin of unburned gas pockets in turbulent detonations," *Acta Astronautica*, Vol. 115, 2015, pp. 40–51. https://doi.org/10.1016/J.ACTAASTRO.2015.05.014.

[31] Gamezo, V. N., Desbordes, D., and Oran, E. S., "Two-dimensional reactive flow dynamics in cellular detonation waves," *Shock Waves*, Vol. 9, No. 1, 1999, pp. 11–17. https://doi.org/10.1007/s001930050134.

[32] Radulescu, M. I., Sharpe, G. J., Lee, J. H., Kiyanda, C. B., Higgins, A. J., and Hanson, R. K., "The ignition mechanism in irregular structure gaseous detonations," *Proceedings of the Combustion Institute*, Vol. 30, 2005, pp. 1859–1868. https://doi.org/10.1016/J.PROCI.2004.08.047.

[33] Ben-Dor, G., *Shock Wave Reflection Phenomena*, 2nd ed., Springer, Berlin, 2007. https://doi.org/10.1007/978-3-540-71382-1.